ASDs of PROTACs: Spray-dried solid dispersions as enabling formulations

Nicole Hofmann [a,b], Meike Harms [a], Karsten Mäder [b,*]

[a] *Global Drug Product Development, Orals Development, Merck KGaA, Frankfurter Straße 250, 64293 Darmstadt, Germany*
[b] *Institute of Pharmacy, Faculty I of Natural Sciences, Martin Luther University Halle-Wittenberg, Kurt-Mothes-Strasse 3, 06120 Halle (Saale), Germany*

ARTICLE INFO

ABSTRACT

Proteolysis targeting chimeras (PROTACs) are a promising class of pharmaceutical agents with a unique mode of action. PROTACs enable the targeting of a broad variety of structures including transcription factors and other "undruggable" targets. The poor solubility and slow dissolution of PROTACs currently limit the extensive use of their potential. Up to date, only very limited drug delivery options have been examined to address this challenge. Therefore, we explored the potential of amorphous solid dispersions (ASDs) by spray drying a model PROTAC with different polymers. The resulting formulations were assessed in terms of purity, solid state, dissolution performance, and stability. A strong increase in supersaturation compared to the physical mixture was provided, although in both systems the PROTAC molecule itself was already in the amorphous state. Evaluation of the reasons for the superiority of the ASD formulations revealed that the major factor was the homogeneous, molecular distribution of the active pharmaceutical ingredient (API) in the polymer matrix, as well as improved wettability of the formulation containing Soluplus compared to the physical mixture. The manufactured formulations were stable over a minimum of 8 weeks when protected from light and humidity.

1. Introduction

Proteolysis targeting chimeras (PROTACs) are a promising new modality, that has gained increasing interest in academia and industry over the past few years. The first PROTAC prototype was developed in 2001 (Sakamoto et al., 2001). By hijacking the cellular disposal system (i.e. the ubiquitin proteolysis system), and thereby degrading proteins of interest (PoI), these compounds emerged as a great opportunity for targeting "undruggable" proteins (Békés et al., 2022; Churcher, 2018; Neklesa et al., 2017). Their mode of action is quite different from the common occupancy-driven model: by inducing proximity between an E3 ligase (which transfers ubiquitin onto lysines) and the PoI and thereby leading to ubiquitination of the protein, PROTACs act as catalytic degradation initiators (Burslem and Crews, 2017; Pettersson and Crews, 2019). In addition to their unique mode of action, adaptation to new targets is relatively straightforward since the PoI targeting moiety can be exchanged easily. These characteristics of PROTACs offer a huge potential for the treatment of different diseases. To recruit both the E3 ligase and the PoI, PROTACs consist of two warheads connected by a linker. Due to this chimeric structure, the resulting molecules usually have a high molecular weight and further unfavorable properties like e. g. poor water solubility. These properties often result in slow dissolution

kinetics and low oral bioavailability (Edmondson et al., 2019; Pike et al., 2020).

So far formulation efforts have been mostly focused on solvent-based approaches (Burslem et al., 2018; Mares et al., 2020) or nanoparticles (Cimas et al., 2020; Fu et al., 2020; Saraswat et al., 2020). Only limited research has been published on enabling drug delivery systems for PROTACs, although several authors have pointed out their importance in bringing PROTACs as promising therapeutic agents to patients (Chen et al., 2022; Yang et al., 2020).

Amorphous solid dispersions (ASDs) are a formulation strategy to address poor solubility and bioavailability of pharmaceuticals. During manufacturing of an ASD, a poorly soluble drug is embedded in a polymeric matrix. Thereby the drug is transferred from the crystalline to the amorphous state and ideally molecularly dispersed in the matrix. In the amorphous form, a molecule is in a higher energetic, enthalpic, and entropic state compared to the crystalline state. The matrix acts as a stabilizer of the amorphous embedded drug during storage and may increase the wettability of the compound (Baghel et al., 2016). Additionally, during dissolution, a suitable polymer serves as a solubilizer and precipitation inhibitor of the dissolved drug. By enhancing the solubility of a drug, the gradient over the intestinal barrier is increased, and passive diffusion is enhanced (Schittny et al., 2020). So far, the

---

* Corresponding author.
  E-mail address: karsten.maeder@pharmazie.uni-halle.de (K. Mäder).

majority of ASD formulations have been developed for crystalline drug molecules (e.g. ketoconazole, fenofibrate). PROTACs are, in contrast to many other drug molecules, often hard to crystallize and most PROTAC molecules are thus in the amorphous state. Therefore, the unusual task emerges to develop an ASD formulation for an amorphous drug molecule. Here, the applicability of an ASD might be different since one of the key steps, namely the amorphization, is omitted. Beneficial attributes of the amorphous state of a drug like higher dissolution rate and higher equilibrium solubility, which contribute to the solubility enhancement, are already demonstrated by the crude amorphous PROTAC that is not embedded in a polymeric matrix. Hence, it is not clear whether an ASD formulation of a PROTAC would provide a higher supersaturation compared to the corresponding physical mixture.

There are numerous manufacturing techniques for ASDs including solvent-based methods like spray drying, coprecipitation, solvent evaporation, and fusion-based techniques like hot melt extrusion, cryomilling, and melt-quenching (Vasconcelos et al., 2016). Among them, spray drying and hot melt extrusion are the most common techniques. In an early development stage, material supply is often limited and the identification of suitable polymers for a stable and functional ASD is crucial. Therefore, several screening and predictive tools for the successful manufacturing of ASDs and the selection from a broad variety of polymers to promising candidates have been developed (He and Ho, 2015).

Polymers may be first classified as either ionic or nonionic. Their respective properties determine the solubility in different biorelevant media. Soluplus is a polyvinyl caprolactam-polyvinyl acetate-polyethylene glycol graft copolymer, that was developed by BASF for hot melt extrusion. In addition, it can also be employed as a polymeric matrix carrier in spray drying. It is neutral and water-soluble regardless of the pH of the medium and has already been implemented in various ASD formulations that provided supersaturation of poorly soluble drugs (Attia et al., 2023; BASF Pharma, 2019). Eudragit E PO is a cationic methacrylate-copolymer usually used for taste masking, that is soluble at low pH values due to a tertiary amine in the structure (Evonik Operations GmbH, 2021). The polymer can be spray-dried and extruded and its value as a polymeric carrier in ASDs has been demonstrated in the literature (Kojima et al., 2012).

The first study on ASDs as a formulation technique for PROTACs was just recently published, where the researchers manufactured ASDs via vacuum compression molding of a von Hippel-Lindau (VHL)-based PROTAC molecule and compared this formulation technique with the liquisolid approach. A solubility enhancement was demonstrated for the formulation of PROTACs as ASDs, whereas no benefit was found for the liquisolid formulation technique in vitro (Pöstges et al., 2023). The crude PROTAC molecule, ARCC-4, was in an amorphous state before the processing. Despite this, formulating it as an ASD showed a strong benefit. Therefore the question arises if other (amorphous) PROTACs would also benefit from the formulation as an ASD in terms of solubility enhancement in biorelevant media. If so, the reason for this and the mechanisms of the supersaturation are still to be investigated.

In the present study, a Cereblon-based PROTAC was chosen, which corresponds to another large group of PROTACs (Bricelj et al., 2021; Ishida and Ciulli, 2021). The used model compound possesses unfavorable properties, which do not comply with Lipinski's rule of five, like a high molecular weight (M_W = 914 Da), high lipophilicity (chromLogD = 7.0), and low solubility in biorelevant media (S_{FaSSIF} = 20 μg/mL). Similar properties are often observed for bifunctional degraders in general, making MS4078 a typical representative of the Cereblon (CRBN)-based PROTAC class (Edmondson et al., 2019). A screening for suitable polymers to prepare binary ASDs of this model PROTAC was conducted. From more than 10 different polymer candidates, two were selected and for the first time ASDs of a CRBN-based PROTAC using different polymers were prepared and the feasibility of their manufacture by spray drying was evaluated. The crude model PROTAC MS4078 (Zhang et al., 2018) was in an amorphous state and so far to the best of

our knowledge, no crystalline structure for the parent compound has been described. The manufactured formulations were compared to the corresponding physical mixture and characterized with a special focus on the supersaturation provided by the two amorphous systems. The decisive differences between the systems were examined by evaluating particle size, API distribution, and wettability. In addition, questions concerning the stability of the formulations at different storage conditions were addressed in this work.

2. Materials and methods

2.1. Materials

MS4078 was purchased from MedChemExpress (USA). Soluplus, Kollidon 30 (K-30) and Kollidon VA64 (VA64) were obtained from BASF (Germany). Eudragit E PO (E PO) and Eudragit L100-55 (L100-55) from Evonik (Germany), different grades of hypromellose acetate succinate (HPMCAS HF, MF and LF), Hypromellose phthalate (HPMCP 50 (HP-50)) from Shin-Etsu (Japan) and cellulose acetate phthalate (CAP) from Eastman (USA). Parteck MXP (MXP) and MXP 3–82 (3–82) were provided by Merck KGaA (Germany). Structures are given in Fig. S1. Hypergrade acetonitrile (ACN) and methanol (MeOH), analytical grade trifluoro acetic acid (TFA), dichloromethane (DCM), dimethylformamide (DMF), and dimethylsulfoxide (DMSO) were produced by Merck KGaA (Germany).

FaSSGF/FaSSIF/FeSSIF powder for the preparation of fasted-state simulated intestinal fluid V1 (FaSSIF) was purchased from Biorelevant (UK). Sodium hydroxide, sodium chloride, sodium dihydrogen phosphate, 1 N hydrochloric acid, and 1 N sodium hydroxide solution for buffer preparation were provided by Merck KGaA (Germany). All aqueous solutions were prepared with purified water (MilliQ (Merck KGaA, Germany)).

2.2. Thermodynamic solubility of the compounds

The thermodynamic solubility was determined by weighing an excess amount of the compound into a vial and adding prewarmed FaSSIF. The suspension was stirred at 37 °C and 300 rpm for 24 h. Samples were withdrawn from the suspension, centrifuged and the supernatant was diluted 1:1 with ACN. Quantification was performed by ultra-performance liquid chromatography (UPLC) (see 2.7.).

2.3. Solvent-based feasibility screen in 96 well plate

A miniaturized solvent-based screening for suitable polymers was performed based on Auch et al. (2018). In brief, 10 mg/mL of different polymers were dissolved in either 90:10 (V/V) DCM/MeOH or DMF. The API was dissolved at 3.33 mg/mL in the respective solvent. An API-polymer solution was prepared containing 90 % (w/w) of polymer and 10 % (w/w) of API in a 96-well plate. DCM/MeOH was evaporated using a desiccator and a vacuum pump (Vacuubrand, Germany), whereas DMF was evaporated using a freeze dryer (Alpha 2–4 LSCplus, CHRIST, Germany). The resulting API-polymer films were assessed under standard and polarized light (IX73, Olympus, Japan, and VHX-7000, Keyence Corporation, Japan). For dissolution testing, 200 μL of FaSSIF and two glass balls were added to each well. After 1 and 2 h of shaking at 37 °C and 700 rpm (ThermoStar, BMG Labtech, Germany), 100 μL were withdrawn and filtered through a 0.45 μm filter plate (AcroPrep™ Advance, Pall Corporation, USA). The filtrate was diluted with the corresponding organic solvent and analyzed by UPLC (see 2.7.). Additionally, stability samples were prepared and stored at 40 °C and in dry conditions via storage in a desiccator over silica gel or at 75 % RH. Visual macroscopic and microscopic assessment as well as dissolution testing were conducted after seven days of storage.

2.4. Manufacturing of formulations

The spray-dried formulations were manufactured using a 4 M8-TriX (ProCepT, Belgium) equipped with a 1 mm nozzle. Solutions with a solid concentration of 2 % (w/w) (10 % (w/w) API and 90 % (w/w) polymer) in 90:10 (V/V) DCM/MeOH were used. Spray drying parameters are summarized in Table 1.

2.5. Manufacturing of physical mixtures

The physical mixtures were prepared by thoroughly mixing the different components with mortar and pestle.

2.6. Stability tests of formulations

The manufactured formulations were stored at 2–8 °C, 25 °C and 40 °C with desiccant and at 40 °C/75 % RH over 8 weeks. At the start and after 4 and 8 weeks, the content and purity of the samples were analyzed by UPLC. Additionally, solid-state was analyzed by differential scanning calorimetry (DSC, see 2.6.1.), X-ray diffraction (XRD, see 2.6.2.) and standard and polarized microscopy using the VHX-7000. In addition, a small-scale non-sink dissolution test was conducted (see 2.6.3.).

2.6.1. DSC and mDSC analysis

DSC and modulated DSC (mDSC) analysis were conducted with a DSC 250 (TA Instruments, USA) which was calibrated for enthalpy using indium and for temperature using tin, indium, 4-nitrotoluol, cyclohexane, and n-octane as references. The calibration is conducted every three months. For conventional DSC analysis, 6–10 mg of the samples were filled into Aluminum pans and closed with a lid. Two cycles of heating and cooling were applied on the unpierced crucibles: up to 190 °C with a heating rate of 10 °C/min and cooled down to −25 °C with a cooling rate of 20 °C/min.

The mDSC analysis was performed with pierced lids. The parameters of the measurements depended on the used polymer and are represented in Table 2.

The glass transition was determined using the TRIOS software (TA Instruments, version: 5.4.0.300). Before and after the step in the heat flow signal (or reversible heat flow, respectively), a tangent was fitted and the glass transition temperature was determined as the half-height midpoint.

2.6.2. XRD analysis

For XRD measurements, samples were prepared on silicon background sample holders without a recess. They were analyzed on a D2 Phaser (Bruker, USA) in a Bragg-Bretano geometry from 6 to 35° 2θ with a step width of 0.02° over a measurement time of approx. 3 h. The samples were rotated at 5 rpm, Cu-Kα radiation (wavelength: 1.54060 Å) was used and separation from Kβ was achieved by a Ni-filter. The measurement was conducted at 30 kV and 10.0 mA, and a 1D-LynxEye served as the detector.

2.6.3. Non-sink dissolution assay

The non-sink dissolution assay was based on Auch et al. (2018) and Gottschalk et al. (2023). Approx. 4.8 mg of sample were weighed into Eppendorf tubes and 1.2 mL of FaSSIF (prewarmed at 37 °C) were added ($c_{MS4078} = 400$ μg/mL). The suspension was vortexed at 1000 rpm for 60 s (Vortex-Genie 2, Scientific Industries, USA) and kept at 37 °C

Table 2
Parameters of mDSC measurements.

Polymer	Amplitude [°C]	Period [s]	Underlying heating rate [°C/min]
E PO	0.4	30	0.5
Soluplus	0.4	30	1.0

(Thermomixer comfort, Eppendorf, Germany) for 2 h without stirring or shaking. 2 min before each sampling point (5, 10, 15, 20, 30, 45, 60, 90, and 120 min) the samples were removed from the Thermomixer and centrifuged for 1 min at 15000 rpm (Mikro 200R, Hettich, Germany). 50 μL of supernatant were withdrawn and diluted with ACN for UPLC analysis (see 2.7.). The remaining suspension was redispersed by a short vortexing period (20 s) at 1000 rpm and placed in the Thermomixer. All samples were prepared in triplicate.

2.7. UPLC analysis

UPLC samples were analyzed using a Waters Acquity H-Class series UPLC system (Waters Corporation, Germany). For the analysis of MS4078 a Waters Acquity BEH C8 column (2.1x50 mm, 1.7 μm) was employed. The mobile phases comprised ACN (Solvent A) and water with 0.1 % (V/V) trifluoracetic acid (Solvent B). Details on the gradient, flow rate, and injection volume can be found in Table S1. A wavelength of 271 nm was used for detection.

2.8. Raman imaging

The spray-dried solid dispersions (SDDs) were pressed into tablets (diameter: 10 mm) with a compression force of 10^5 N using a semi-automatic press PE-010 (Mauthe Maschinenbau, Germany). Raman mapping was conducted on an Apyron confocal Raman microscope (WITec, Germany) equipped with Zeiss microscope objectives (Zeiss, Germany). The samples were assessed with ~ 100x magnification using a 785 nm laser with a power of 70 mW and 0.3 s (Soluplus) or 0.4 s (E PO) integration time. Mapping was done on a rectangle of 10 x 20 μm with 60 x 90 (Soluplus) or 30 x 80 points (E PO) of acquisition. Smoothing of the spectra was done using 10 neighbors on each side and a second-order polynomial by the method of Savitzky and Golay (Savitzky and Golay, 1964).

2.9. Electron microscopy and energy-dispersive X-ray spectroscopy (EDS)

For the scanning electron microscopy (SEM) a VEGA3 XMU (TESCAN, Germany) equipped with a wolfram cathode was used. The measurements were conducted at ~ 800x magnification and an accelerating voltage of 15 kV. Energy dispersive x-ray spectroscopy (EDS) was carried out on a Bruker Quantax 800 with a silicone drift detector (XFlash 6/60, Bruker, Germany). The elemental mapping was done on tablets prepared from the spray-dried formulations (see 2.8.) for either 23 min (Soluplus) or 56 min (E PO). An area of 333 x 250 μm was measured with 800 x 600 points of acquisition.

2.10. Tablet production for wettability tests

The parameters for the production of tablets of the neat API, neat polymers, SDD formulations, and physical mixtures with 75 %, 50 %, 25 %, and 10 % (w/w) of drug load were developed. Tablets were produced on the Texture Analyzer (TA.Xtplus, Winopal, Germany) and Gamlen

Table 1
Spray drying parameters of formulations containing MS4078.

Polymer	API	T_{in} [°C]	T_{out} [°C]	Air speed$_{Chamber}$ [m³/min]	Air speed$_{Cyclone}$ [m³/min]	Airflow $_{nozzle}$ [L/min]
E PO	MS4078	70	36–38	0.3	0.1	10
Soluplus	MS4078	80	40–42	0.3	0.1	8

D500 (Gamlen Tableting Ltd, UK). The maximum compression load of the Texture Analyzer (50 kg) was not sufficient to produce tablets (diameter 4 mm) from the neat API. Higher compression loads could be applied using the Gamlen D500 equipped with a 500 kg load cell. The parameters were optimized to obtain tablets that were robust enough to enable manual handling. Compression load and speed needed to be reduced to prevent excessive friction and heat generation. The tablets were prepared for wettability tests. Different contact angles and spreading of the droplet on the tablet surface were observed. The diameter of the tablets had to be adjusted to avoid rim effects during wettability tests. Finally, 35 mg of the respective powder was filled into a 6 mm die and compressed with a load of 200 kg. Each tablet was checked for defects under the microscope before further use.

2.11. Wettability tests

The tablets (see 2.10) were conditioned for at least 2 h at room temperature (~20 °C) and 60 % RH which was realized in a chamber with saturated NaBr solution (Greenspan, 1977). For the measurements, 5 μL of MilliQ-water was automatically pipetted onto the tablet and analyzed over 3 minutes by a DSA25S (Krüss, Germany). The Young-Laplace fitting routine of the internal software (Advance, version: 1.15.0) was used for analysis.

3. Results

3.1. Thermodynamic solubility

For information about the pure compound, the thermodynamic solubility after 24 h of MS4078 was determined in FaSSIF at 37 °C and was found to be 20.21 ± 0.05 μg/mL.

3.2. Solvent-based feasibility screen

To identify suitable polymeric carriers for MS4078, a small-scale screening was conducted. The results of the solvent-based feasibility screens of MS4078 including the stability samples are depicted in Fig. 1. The API reference sample of MS4078 had a solubility of ~ 10 μg/mL confirming the poor solubility of the neat amorphous API. Compared to the thermodynamic solubility of the API, a slightly reduced

concentration was dissolved during the assay, probably due to a slow dissolution rate of the compound. Most polymers could not provide a benefit, but Soluplus, E PO, MXP, and 3–82 resulted in a high supersaturation of up to 50fold compared to the solubility of the pure API. Concentrations found at the second sampling point (after 2 h), were either similar compared to the results from the first sampling point, or increased (Soluplus), hence, the supersaturation was stabilized over the time of the assay. The promising films were also prepared for stability testing: they were stored for seven days at 40 °C and either under dry (with desiccant) or humid conditions (75 % RH). A reanalysis of the solid-state was conducted after seven days by polarized microscopy (PolMic), and dissolution performance was tested in FaSSIF. The microscopic assessment revealed no changes – neither phase separation nor crystallization was observed (Fig. S2). The results of the dissolution test (Fig. 1) after one week of storage were very similar to the start values, regardless of the storage condition.

3.3. Spray dried formulations

For spray drying, Soluplus and E PO were chosen as carrier systems, and binary formulations containing 10 % (w/w) of MS4078 and 90 % (w/w) of either Soluplus or E PO were successfully prepared. Content and purity were checked by LC and matched the requirements of 95–105 % and > 98 %, respectively. Yield accounted for > 65 % in the case of Soluplus and > 80 % in the case of E PO. Formulations with MXP and 3–82 have not been sprayed due to the poor solubility of the polymers in volatile solvents. However, they might be promising polymers as well.

3.4. Analysis of formulations and physical mixtures

The formulations and physical mixtures were analyzed with a focus on their dissolution performance. As the formulation and the physical mixture comprise the same compositions, the goal of this assay was to elucidate the impact of the processing step on the supersaturation and its kinetics. Additionally, solid state and particle size were determined as both depend on the processing step and also impact the dissolution process. Fig. 2 shows the results of a non-sink dissolution assay in FaSSIF of the spray-dried formulations (SDD) in contrast to the physical mixtures (PM) and the crude API. The pure API dissolved rapidly and exhibited a maximum of 9 μg/ml after 5 minutes. Afterwards, the concentration decreased promptly, indicating a precipitation of the API from the solution. In contrast, the physical mixtures did not show a maximum at the first sampling point but rather a slow increase in concentration over the assay (Fig. 2C, Fig. S3). The concentration at 5 minutes was lower for the PM than for the crude API, however, due to the large error bar for the crude API (most likely caused by the fast dissolution kinetics and the subsequent rapid precipitation) this is not significant. In most cases for ASDs, the maximum in supersaturation is reached faster than observed here, where it increases over the full two hours. This might be caused by the dissolution of the polymer being the rate-limiting step. The general results of the screening experiment of MS4078 were confirmed by the SDD formulations: With > 70fold a high supersaturation compared to the crude API was found for both polymers with values > 280 μg/mL after 2 h. The physical mixtures exhibited only a slight improvement with 3fold (Soluplus) and 10fold (E PO) higher concentrations.

The amorphous state of the crude API and all formulations was confirmed by DSC, XRD, and PolMic. XRD data are given in Fig. 3. The API and the polymers as well as the formulations after manufacturing and after storage showed no crystalline signals over the scanned range (2θ = 6-35°). The absence of reflexes in the XRD analysis indicated an amorphous state of the sample. This result is in accordance with DSC analysis: Here, for the neat API, no melting point could be determined but a glass transition with a relaxation enthalpy around 100 °C confirming the amorphous state of the API (Fig. S4). However, DSC and
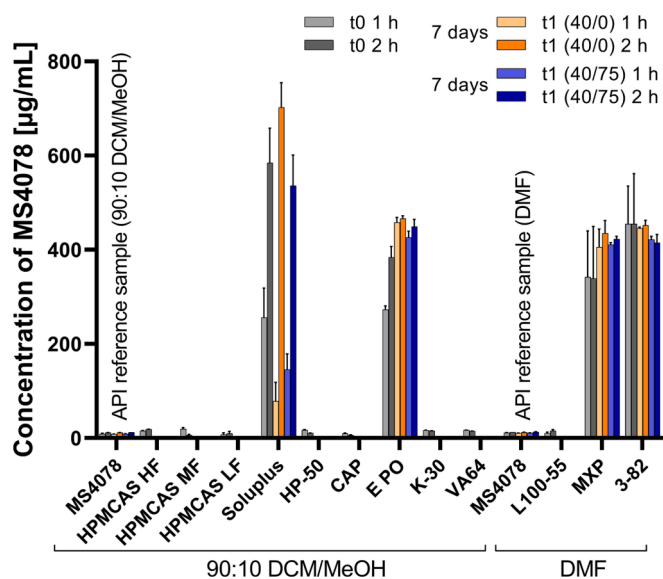
Fig. 1. Dissolution results of the solvent-based feasibility screen of MS4078 in FaSSIF at start (t0) and after storage for 7 days at 40 °C and dry conditions (t1 40/0) and 40 °C/75 % RH (t1 40/75). (Mean ± SD (n = 3)).
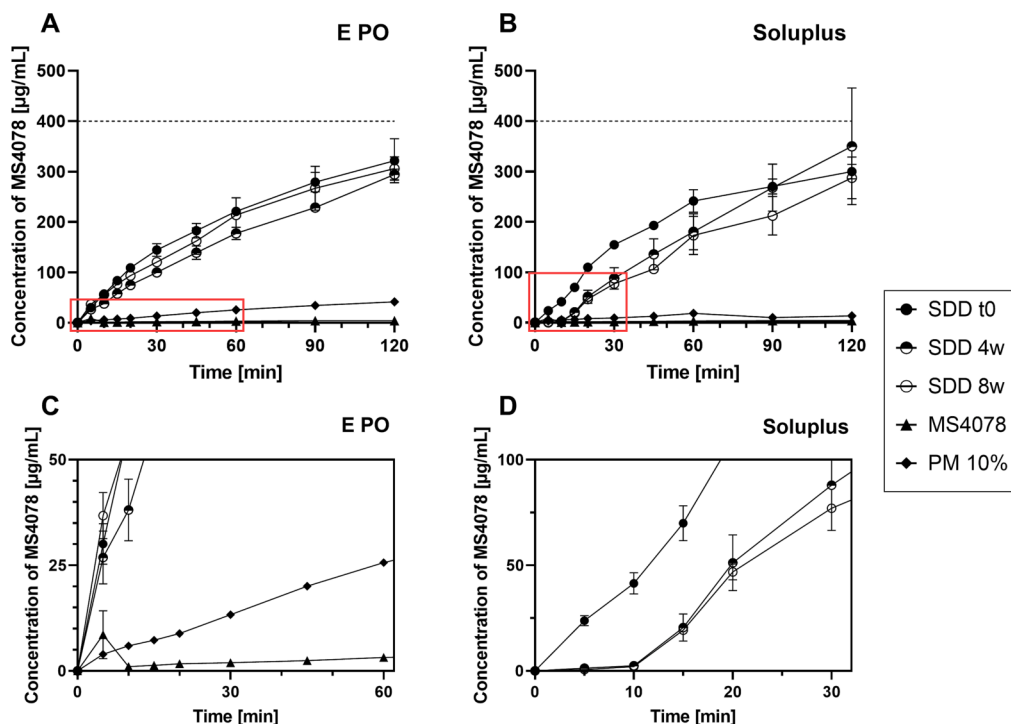
Fig. 2. Dissolution in FaSSIF of the SDDs at start (t0) and after 4 and 8 weeks of storage at 40 °C/75 % RH and their corresponding PMs of A) E PO and B) Soluplus in comparison to crude API (MS4078). The dashed line at 400 µg/ml represents the 100 % dissolution. C) Magnification of the first 60 min of the dissolution results of MS4078, PM-E and SDD-E. D) Magnification of the first 30 min of the dissolution results of SDD-S. (Mean ± SD (n = 3)).
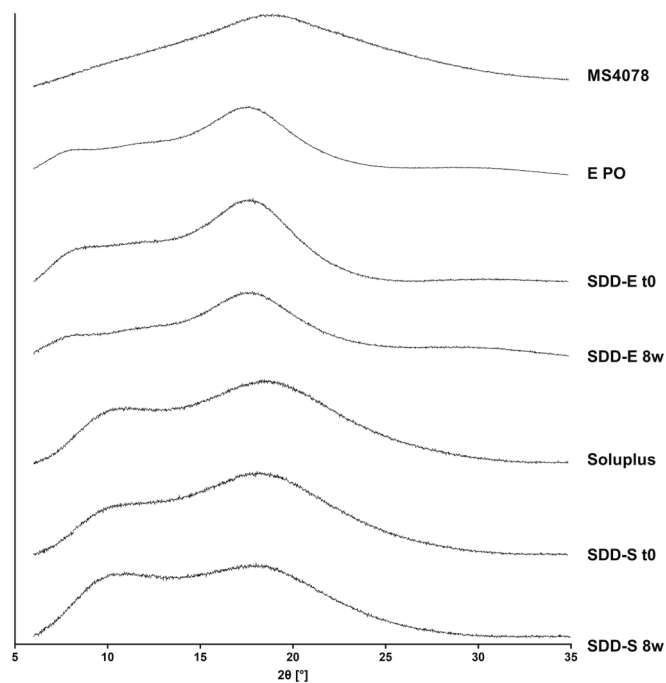
Fig. 3. X-ray diffraction patterns of E PO, MS4078, Soluplus and SDD-E and SDD-S at start (t0) and after 8 weeks of storage at 40 °C/75 % RH.

mDSC measurements of the formulations and PMs were not conclusive regarding the homogeneity of the manufactured formulations: DSC data revealed a glass transition around the same temperature as the neat polymers. However, at temperatures > 100 °C thermal events were observed that could not be assigned to glass transitions, melting points, or other determined thermal events. Therefore, a modulated DSC

analysis was conducted, to better separate the thermal events and identify whether multiple glass transitions were present. Several steps were found for neat E PO, which were also present in measurements of the physical mixture (PM-E 10 %). The crude API also exhibited various steps – most of them in the same temperature range as the steps of E PO (Fig. S5). This coincidence prevents a differentiation between a single and multiple-phase system. In the case of neat Soluplus, a single T_g was found at ~ 110 °C. However, the analysis of the physical mixture did not reveal different steps, but only one broad T_g (Fig. S5). Therefore, no conclusions about homogeneity could be drawn from the DSC and mDSC measurements.

The particle size of the SDD formulations was determined by microscopy where the largest extension of an individual particle served as the size. The diameter was between 1 and 20 µm (SDD-E) and 2–35 µm (SDD-S), whereas 2–30 µm (PM-E 10 %) and 10–100 µm (PM-S 10 %) were found for the physical mixtures. The spherical SDD particles had a slightly yellow and homogeneous color. In the PMs the polymeric and API particles could be clearly differentiated by their colors in the microscopic image: yellow particles of MS4078 and white particles of E PO or Soluplus (Fig. S6).

Storage stability of the formulations was carried out for both SDD formulations at different temperatures (2–8 °C, 25 °C and 40 °C) under dry conditions and additionally under humid, accelerated conditions (40 °C/75 % RH). For both polymers, a decrease in purity of MS4078

Table 3
Purity of SDD-E and SDD-S at the start (t0) and after 8 weeks of storage under different conditions.

Condition	SDD-E Purity [%]	SDD-S Purity [%]
t0	98.6	98.9
8w 2–8 °C	98.4	98.8
8w 25 °C	98.1	98.8
8w 40 °C	97.3	98.8
8w 40 °C/75 % RH	82.9	97.1

was observed under humid conditions accompanied by agglomeration or fusion of the particles (Table 3, Fig. S6). The agglomeration can be explained by the hygroscopicity of the polymers: due to water incorporation the mobility of the molecules was increased since water has a plasticizing effect. This effect combined with the elevated storage temperature promoted the fusion of the particles. Under dry conditions at the same temperature (40 °C), a decrease in purity was also observed for SDD-E but was much less pronounced compared to the humid conditions. For all other samples, purity remained high and similar to the start value (Table 3). No changes were noted in solid state analysis, even after storage under accelerated conditions (40 °C/75 % RH). Instead, only an amorphous halo was found after 8 weeks (Fig. 3) and this finding was complemented by the absence of birefringence under polarized light (Fig. S6). The dissolution performance was not affected by storage in the case of SDD-E; however, SDD-S exhibited a pronounced lag time in the first few minutes of the dissolution assay after storage at 40 °C/75 % RH. Nevertheless, more than 250 µg/mL of MS4078 were dissolved after 120 min, matching the results from the start analysis (Fig. 2).

3.5. EDS elemental mapping and Raman imaging

A rather obvious difference between the SDD and the physical mixture is the API being more or less homogenously dispersed in the polymeric matrix in the SDD while they are located in separate particles in the PM. As this may be a reason for the improvement in supersaturation for the SDD, Raman and EDS elemental mapping were performed. With these analytical techniques, the distribution of the PROTAC in its polymeric carrier can be evaluated as they allow spatial resolution between the API and polymers at least down to micrometer-sized clusters.

An overview of the API distribution on tablets prepared from SDD-E and SDD-S was obtained by EDS elemental mapping. Each point (pixel size: 416 nm) over an area of 333 x 250 µm was analyzed. The characteristic elements are chloride and sulfur, which are present in MS4078 but not in the structures of the polymers (Fig. S1). Both elements scatter at higher X-ray intensities which are well resolved in contrast to elements with lower atomic numbers (C, N, O). In Fig. 4 the SEM pictures, spectra of both measurements, and the distribution of Cl and S are displayed. From the distribution of Cl and S atoms, no large clusters could be identified, indicating a one-phase system and a homogeneous distribution of the API in the polymeric matrix. Tablets prepared from the PMs were not analyzed since clusters of polymer and API could be differentiated already in microscopic images taken at 20x magnification. Pictures of tablets prepared from SDD powder and physical mixtures are given in the Supplementary information (Fig. S7).

A more detailed analysis of the distribution of MS4078 was done after mapping an area of 10 x 20 µm and evaluating the obtained Raman spectra. A heat map of the API and the polymer distribution was obtained. In Fig. 5 these heat maps are displayed and the spectra of the points where a minimum of the API was detected as well as the spectra where a maximum of the polymer was identified.

In the case of E PO, the most intense peak at 1446 cm^{-1} is characteristic of the polymer, whereas the peak at 1614 cm^{-1} is only present in the spectrum of the API (Fig. 5D, marked area). In regions where minimum API was detected, a clear signal was still visible from the API (Fig. 5C). The same applies to the maximum spectra of E PO, where a
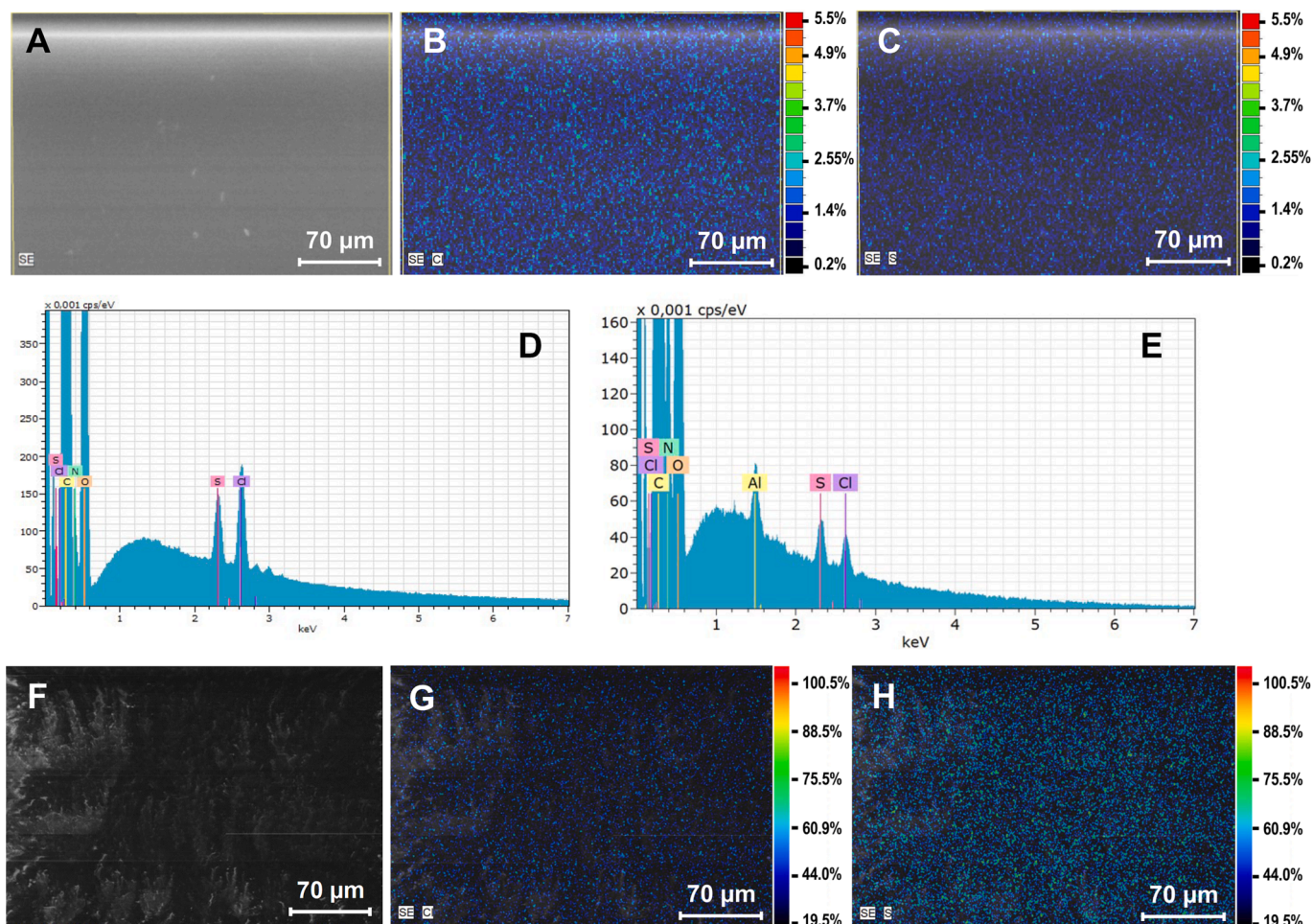
Fig. 4. SEM pictures of SDD-E (A) and SDD-S (F). EDS spectra of SDD-E (D), SDD-S (E), and distribution of Cl and S in SDD-E (B, C) and SDD-S (G, H).
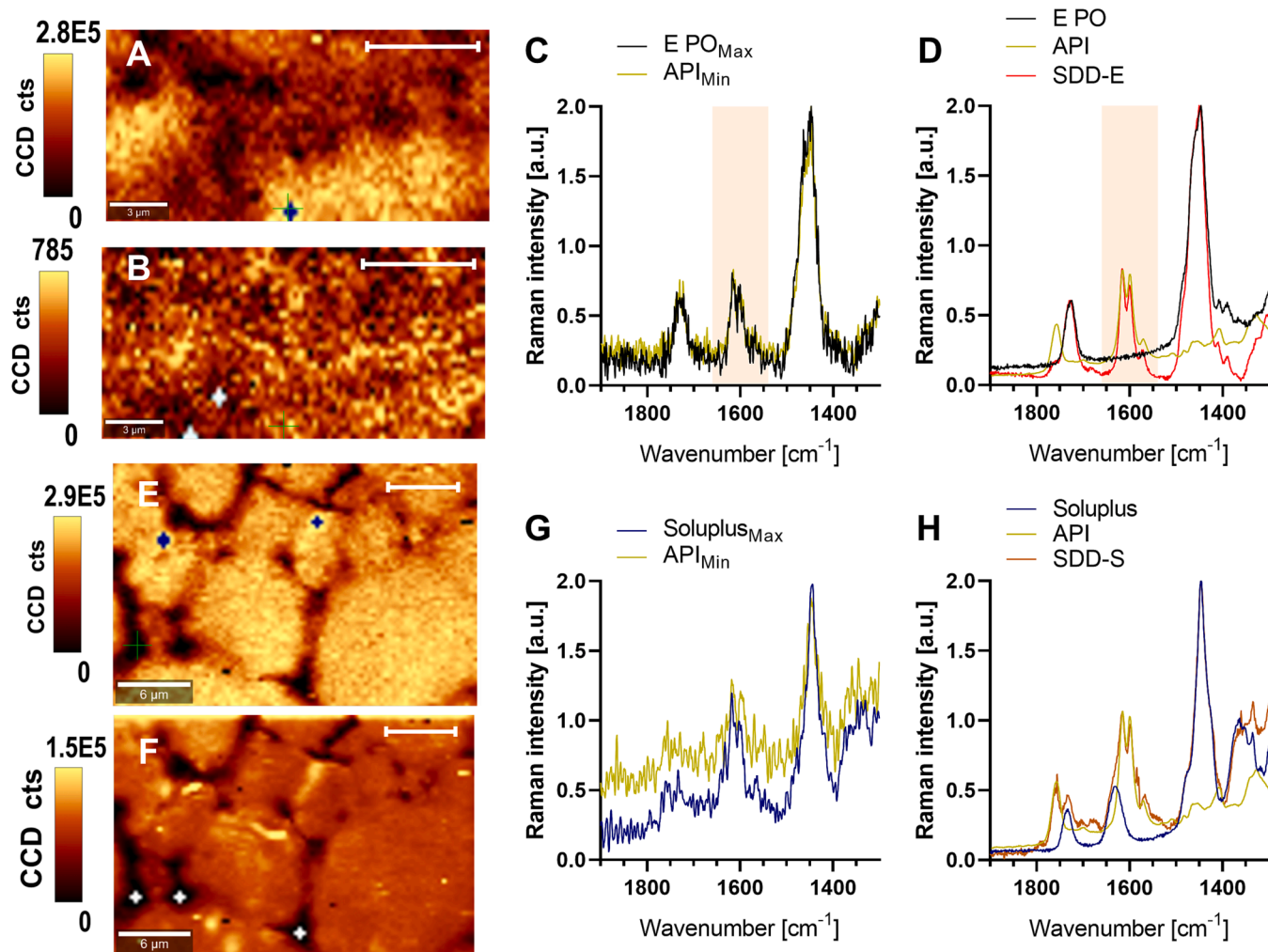
Fig. 5. Heat maps of polymer and API distribution of SDD-E (A: Polymer, B: API) and SDD-S (E: Polymer, F: API). The scale bar (top right corner) is 6 μm. Raman spectra at the position of a minimum signal of API or a maximum of polymer (C: SDD-E (original) and G: SDD-S (smoothed)). Locations of min and max spectra are indicated by white and dark crosses on the heat map. Average Raman spectra of SDD-E and SDD-S over the entire area compared to Raman spectra of polymer and API (D, H).

peak representative of the API was also found. Both observations indicate that minor variations in the content were detected. Besides, since no clusters are visible in the heat maps, it can be concluded that the API is homogeneously distributed according to the resolution of Raman microscopy ($\sim$0.25 μm).

The spectra of Soluplus and MS4078 overlap to a huge extent. The most intense peak of Soluplus at 1446 cm^{-1} and the second most intense peak at 699 cm^{-1} are the two points from which the presence of the polymer can be identified. For the API however, there was only one peak at 1757 cm^{-1} that identified the API. On the other hand, a peak at 1733 cm^{-1} was also found in the Soluplus spectrum, resulting in a double peak in the combined spectrum (Fig. 5H and Fig. S8). The two heat maps of the API and Soluplus distribution show a similar picture, that the regions of minimum API signal were also minimum signals of Soluplus (Fig. 5E, F). This is an important observation since an opposed picture would indicate different phases. The reason for this clustering of high signals and low signals is most probably based on the surface topography of the sample. From the heat map, the particle shape can be estimated (high signal), whereas the area between "particles" is an area of low signal. Hence, the points of the minimum signal were probably out of focus. Thus, the spectra of the minimum signal of the API and the maximum signal of Soluplus are very noisy, which is solely caused by the surface roughness. Therefore a differentiation between a single or a double peak around 1740 cm^{-1} was not possible (Fig. S8). An alternative approach is

to use the most intense peaks of the API (double peak at 1599 cm^{-1}/1615 cm^{-1}). However, they overlap with a rather small peak of Soluplus (maximum: 1630 cm^{-1}). An intense peak is also visible in the minimum and maximum spectra. For a better evaluation, the ratio of the most intense polymer peak ($\sim$1445 cm^{-1}) and the most intense API peak at $\sim$ 1599 cm^{-1} was calculated from smoothed data (Fig. 5G and Table 4, the graphs of the corresponding original spectra can be found in the Supplementary information (Fig. S8)). Based on the intensity ratios, it can be concluded, that the signal originates from the API. All in all, this proves – just like for E PO – that the API and Soluplus do not form clusters in the lower micrometer range.

Raman mapping of the tablets confirmed the findings from the EDS measurement: both analysis techniques indicated a one-phase system and a homogeneous distribution of MS4078 in the polymer matrices of SDD-E and SDD-S within their corresponding resolution ($\sim$1 μm).

Table 4
The intensity ratio between the maximum at $\sim$ 1599 cm^{-1} and the maximum spectrum ($\sim$1445 cm^{-1}) was calculated from smoothed Raman spectra.

Spectrum	Soluplus	SDD-S (average)	Soluplus$_{Max}$	API$_{Min}$
Ratio	0.11	0.49	0.51	0.64

3.6. Wettability tests

An often-discussed principle for the improvement in dissolution kinetics for ASDs is improved wettability (Matteucci et al., 2008; Schittny et al., 2020). Therefore, differences between the PMs and the formulations in terms of wettability were examined by measuring the contact angle of water on tablets of the crude API and polymers, physical mixtures as well as SDDs. The results of the wettability tests are given in Fig. 6.

Video recording and picture evaluation started immediately after 5 μL was dropped onto the tablet. The drop settled within the first 0.5 s on the tablet surface. Over the test period (3 min) a decrease of the contact angle was observed. In the case of E PO, the PM-Es, MS4078, and SDD-E the contact angle hardly changed after 0.6 s ($< 6°$), and for pure Soluplus and SDD-S, the change remained small ($< 9°$). However, for the different PMs of Soluplus, larger differences between the start value of the contact angle and the end were found. The differences in contact angle over 3 minutes are possibly based on dissolution of the polymer and the API and thus an alteration of the surface tension due to solubilizing effects. Additionally, solubilization may change the surface roughness and capillary forces that indirectly impact wettability as well. In contrast to E PO and MS4078, Soluplus is water-soluble, thus the polymer probably dissolved faster and to a larger extent resulting in a more pronounced effect. Interestingly, the decrease in contact angle of the physical mixtures correlated with increasing drug load and reached a difference of ~ 40° (PM-S 75 %) between the start and after 180 s. This unexpected observation can be explained by capillary forces, since smaller amounts of Soluplus, the fast-dissolving part of the tablet, have a similar effect to disintegrants (Fig. 6 and Fig. S9). So, the water is drawn into the tablet resulting in a fast decrease of the contact angle. To exclude the effects from dissolution, only the values at t=~0.6 s were used for the evaluation of the contact angle, such that no polymer or only a negligible amount was dissolved in the water droplet and diffusion to the surface had not yet taken place (Fig. 6A).

The wettability of the crude API was poor and in comparison, E PO had a slightly smaller contact angle (i.e. better wettability). No difference could be found between E PO or the PMs and SDD-E, which may be due to the small difference in wettability of the pure compounds. Soluplus exhibited the smallest contact angle, hence wettability of the pure polymer was best. Here, the contact angle increased with the increasing drug load of the physical mixtures. Comparing SDD-S with the PM of the same drug load (10 %), a difference could be seen: The contact angle of SDD-S was similar to the one of the pure polymer whereas the wettability of PM-S 10 % was poorer. These observations indicated that in SDD-S the properties of the polymer dominated while in the PM-S the less evenly distributed poorly wettable API had a stronger impact.

4. Discussion

Amorphous solid dispersions are often used to improve the solubility and thereby the bioavailability of poorly soluble compounds of BCS class II and IV. However, these compounds are usually crystalline, thus, their solid state is altered in the process. The resulting amorphous compounds or formulations possess a higher entropic and enthalpic energy relative to the crystalline ones. Beneficial attributes of the amorphous compared to the crystalline state are increased solubility, wettability, and dissolution kinetics (Baghel et al., 2016). However, there are some examples where amorphous compounds were successfully embedded into polymeric matrices and the resulting ASDs also provided a solubility enhancement (Krome et al., 2020). Furthermore, in a recent paper by Pöstges et al. (2023), the first PROTAC compound was formulated as an ASD by vacuum compression molding (VCM). The solubility of this amorphous VHL-based PROTAC was enhanced by the formulation. In contrast to the previously published work, in our study, a Cereblon-based PROTAC was used as a model API with representative properties as discussed in the introduction section. To explore further formulation techniques apart from VCM, spray drying was chosen to produce binary ASDs, since it is one of the most commonly used approaches.

At first, suitable polymeric carriers that would provide a supersaturation in biorelevant media had to be identified. Therefore a miniaturized screening by preparing API-polymer films, analyzing them via PolMic, and conducting a dissolution test in FaSSIF, was carried out. The screening resulted in several hits with Soluplus, E PO, and PVAs (MXP and 3–82) as very promising polymeric candidates due to high and stable supersaturations. Compared to the neat compound up to 50fold supersaturation could be achieved. Homogeneous, amorphous solid dispersion films were obtained in the screening experiment, as can be seen from the microscopic assessment under standard and polarized light. A 1-week stress test at 40 °C under dry and humid conditions revealed no changes in the films (Fig. 1 and Fig. S2). Based on these results Soluplus and E PO were chosen for a spray drying feasibility. An amorphous formulation of both polymers in combination with 10 % MS4078 each was successfully produced (Fig. 3) and > 65 % yield was obtained after drying. Both binary ASDs were tested for their dissolution performance, which confirmed the observed strong supersaturation in the screening experiment (Fig. 2).

As mentioned before, the alteration of the solid state from crystalline particles to amorphous particles with advantageous properties is usually named one of the key elements of solubility enhancement by ASDs. However, in the special case of PROTACs, the model compound in this study, as well as the VHL-based PROTAC from the first ASD paper of PROTACs, were both amorphous (Pöstges et al., 2023). As the API is in an amorphous state even in the PM (Fig. 3), a supersaturation effect only caused by the polymers might be observable. The pure amorphous API dissolved very fast, resulting in a supersaturated solution at the first sampling point (5 minutes). A decrease in concentration was observed at the next sampling point, indicating that the supersaturated state was not stable and MS4078 had precipitated. This was not observed for the physical mixtures, where a slower increase (but not significant) in concentration was measured, but no decrease by precipitation was detected (Fig. 2C, Fig. S3). Nevertheless, the physical mixtures provided
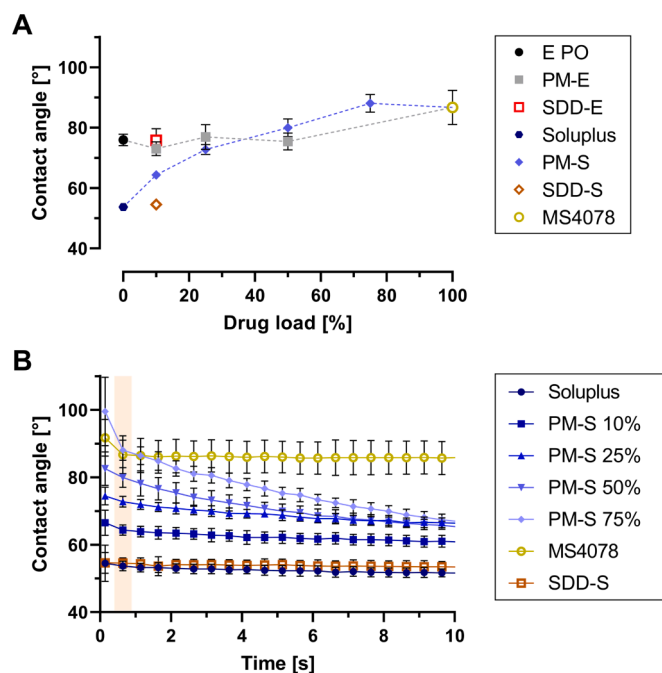
Fig. 6. A) Contact angle of a water droplet on tablets of E PO, Soluplus, corresponding PMs, MS4078, SDD-E and SDD-S after ~ 0.6 s. B) Contact angle of Soluplus, corresponding PMs, MS4078, and SDD-S over 10 s. Contact angles in marked areas are also displayed in A. (Mean ± SD (n = 9–12)).

a slight supersaturation of 10fold (PM-E 10 %) or 3fold (PM-S 10 %) compared to the crude API which is most likely caused by a solubilizing and stabilizing effect of the polymers. In contrast, compared to physical mixtures of the same composition, a distinctive effect of the SDDs was shown. The SDDs achieved in both cases an increase of the API concentration of more than 70fold. In all instances, no precipitation was observed, hence, the dissolved polymer was able to stabilize the higher amounts of MS4078 in solution. Putting all the aspects together, a benefit was obtained from both the physical mixture and the SDD formulations. However, the solubilization by the polymer cannot be the only reason for the supersaturation provided by the SDDs (Fig. 2). Thus, further experiments were conducted to elucidate whether wettability, particle size, or distribution of the API in the polymeric matrix were the elements of the superior performance of the binary ASDs.

The wettability of a powder can be influenced by several factors. Due to interactions between different constituents of the powder, the wettability can be greatly affected (Dahlberg et al., 2010). During dissolution, wetting influences the dissolution performance and dissolution rate to a great extent (Chokshi et al., 2007; Efentakis et al., 1991). Consequently, the wettability may impact the supersaturation of the ASDs and PMs. To evaluate this factor, contact angle measurements of tablets prepared from the SDDs, PMs, and crude API and polymers were conducted. The transfer from the crystalline state to the amorphous state can change the surface energy by exhibiting more polar groups due to the disorder in amorphous solids compared to their crystalline counterparts (Puri et al., 2010). In our case, the comparison of equally amorphous physical mixtures and spray-dried formulations should not influence the exposed groups whereas incorporation of the compound into a better wettable excipient could lead to changes in the wettability. As can be seen in Fig. 6, the wettability of the API was poor compared to the neat polymers. To differentiate, PMs with increasing drug load were prepared to evaluate the effect of a larger proportion of MS4078 on the contact angle. In the case of E PO, the difference between API and neat polymer was small and all PMs had a similar contact angle to the neat polymer. Besides, no difference was found between the SDD and PM-E 10 %. In contrast, increasing the drug load of the PMs led to an increasing contact angle and thus, poorer wettability in the case of Soluplus. Comparing SDD-S and PM-S 10 %, the PM exhibited a higher contact angle (i.e. poorer wettability). Consequently, better performance of SDD-E over PM-E 10 % cannot be explained by improved wettability, whereas for Soluplus it might have a positive impact.

One of the differences between the PMs and the SDD formulations in this study was the particle size. Particles manufactured by spray drying are usually spherical and have a size in the lower micrometer range. The two SDD formulations consisted of spherical particles with a size of < 20 μm (SDD-E) and < 35 μm (SDD-S). The particles of the physical mixture were irregular and larger (< 30 μm (PM-E) and < 100 μm (PM-S), Fig. S6). The particle size plays an important role in dissolution kinetics (Dokoumetzidis and Macheras, 2006). An impact on the supersaturation has only been observed for rapidly crystallizing compounds, where the drug crystallized during dissolution which consequently impaired the supersaturation from the ASD (Matteucci et al., 2008). Nevertheless, this factor was investigated in this study to exclude if the difference in particle size between PMs and SDD formulations would have an impact on the supersaturation. The influence of the particle size could be derived from the stored samples. After storage at 40 °C/75 % RH agglomeration of the particles of SDD-E was observed (Fig. S6). However, the dissolution performance was not affected by storage. Small differences were found for Soluplus, where the maximum concentration was not affected by the extreme increase in particle size over storage, but only the dissolution kinetics. In the beginning, a lag time over the first 10 min was observed, but afterward, the concentration of MS4078 rose quickly, and at 120 min a similar supersaturation to the freshly prepared samples was reached (Fig. 2). The difference can be explained by the particle size. In the case of SDD-E, the particles agglomerated whereas particles of SDD-S fused completely due to storage under high humidity (Fig. S6).

Therefore, the API and polymer needed to be dissolved from particles of SDD-S in the 100 μm (or even larger) range. For E PO only the agglomerates had to be dispersed so that the dissolution itself could take part from the original fine particles (1–20 μm in diameter). In both instances, the particles in the PMs were larger than those of the spray-dried formulations, but not larger than the fragments of SDD-S after storage under humid conditions. According to the Noyes-Whitney equation (Bruner and Tolloczko, 1900; Dokoumetzidis and Macheras, 2006), dissolution kinetics depends on the surface area of the particles and the thickness of the diffusion layer. Hence, the larger a particle, the smaller the overall surface area of a certain amount of powder and the thicker the diffusion layer, resulting in slower dissolution from large particles. The results from the stored SDD-S samples complied with this rule. Overall, these tests demonstrated that the supersaturation was not affected by particle size or surface area, but the dissolution kinetic was dependent on these factors.

Another difference between the physical mixtures and the spray-dried formulations was the distribution of the API. As discussed in detail elsewhere (Chen et al., 2016; Schittny et al., 2020), a homogeneous distribution of the API in the polymeric matrix is one of the crucial points of the functional supersaturation stabilization of ASDs. It has been demonstrated that the inhomogeneous distribution of the API could outweigh strong interactions between the individual constituents and hamper supersaturation.

Detection of different phases in DSC analysis is possible for domains as small as ~ 30 nm, making it a very sensitive analysis technique. However, this only applies given a high ΔC_p (heat capacity), sufficiently high ΔT_g between the glass transitions of the two constituents, and at least ~ 20 % of the sample to be phase separated (Padilla et al., 2011). Unfortunately, DSC and mDSC results were not conclusive in this study and it was not clear, whether the API was homogeneously distributed in the matrix. One of the reasons aside from similar positions of the thermal events in the DSC and mDSC analysis may be the drug load of 10 %. Sensitivity might be an issue at low drug loads for the detection of multiple phases. As investigated and discussed elsewhere (Qian et al., 2010), relying solely on DSC analysis is not always sufficient to detect phase separation and a combination of methods is more suitable to clarify this question. Therefore, Raman and EDS were chosen as complementary methods to evaluate phase separation. By energy dispersive spectroscopy, an overview of the API distribution was taken from a tablet surface: Here, an area was mapped and the distribution of S and Cl was considered to give a rough distribution of the API. According to this method, both elements were randomly distributed and no clusters with or without the two elements were found at a magnification of $\sim 800x$ (i. e. a pixel size of 416 nm) (Fig. 4). Hence, a homogeneous distribution of MS4078 can be assumed in SDD-E and SDD-S. Zooming in, Raman mapping was done on a smaller cutout to evaluate the distribution of the polymer and the API with higher resolution (~ 0.25 μm). From the heat maps and the evaluation of the areas with a minimum of MS4078 or a maximum of the polymers, a homogeneous distribution of the API was confirmed in both formulations (Fig. 5). Due to the resolution of the two analytical techniques, no conclusions could be drawn for clusters with a size < 1 μm. In comparison, the particle sizes of the API and the polymers accounted for 5–30 μm (API, PM-E), 7–20 μm (E PO, PM-E), and 10–50 μm (API, PM-S) and 10–100 μm (Soluplus, PM-S), respectively (Fig. S6). Consequently, the API was distributed on a finer scale in the SDD formulations as shown by EDS and Raman. As described in the last passage, the homogeneity of an ASD formulation is one important factor in supersaturation stabilization. In addition, the release of polymer and API during dissolution is also influenced by the distribution in the polymeric matrix (Baghel et al., 2018; Schittny et al., 2020). The interplay of these two factors finally enables the increased stable supersaturation. Therefore the homogeneous distribution of MS4078 in the polymeric matrices is most probably one of the decisive factors for the superiority of the SDD formulations over the amorphous PMs.

Instabilities of ASDs are a huge drawback, that can be detrimental to

this formulation approach. Phase separation and consequently, recrystallization of the compound are challenges, that can be addressed by choosing a suitable polymeric carrier (He and Ho, 2015). For the evaluation of instabilities, stability tests under different storage conditions are necessary. In the special case of PROTACs or other amorphous compounds, that are hard to crystallize, recrystallization might not occur but other instabilities, like chemical degradation of the compound or phase separation, that consequently affect the dissolution behavior. As discussed in the previous passages, a homogeneous distribution of the API is possibly the decisive parameter that influences dissolution performance. Therefore, the manufactured SDD formulations were additionally stored over eight weeks. The samples were kept at 2–8 °C, 25 °C and 40 °C protected from humidity and in addition, one sample was stored at 40 °C and 75 % RH to evaluate accelerated conditions and humidity stress. At several time points, purity, as well as solid state by XRD and polarized microscopy was checked and the dissolution performance was evaluated. Storage under humid conditions led to agglomeration (SDD-E) or fusion (SDD-S) of the fine particles (Fig. S6) and the purity of the compound was negatively affected (Table 3). However, the overall supersaturation was not impaired and even from the large particles of SDD-S, similar concentrations were stabilized as from freshly manufactured formulation, although the dissolution kinetics were slower due to reduced surface area compared to the originally fine particles (Fig. 2). The evaluation of the solid state of the highly stressed samples indicated no differences by XRD and PolMic (Fig. 3 and Fig. S6). The samples stored under dry conditions did not reveal any changes in solid state or dissolution performance (data not shown) and purity remained high, similar to the start value (Table 3). The observations made during the dissolution assay do not indicate a phase separation during storage, since supersaturation remained high. Overall, the formulations are stable over the tested time under dry conditions. In contrast, under humid conditions, degradation of the compound but no physical instability impacting the supersaturation was observed. Therefore it is imperative to store the formulations protected from humidity.

5. Conclusion

Amorphous solid dispersions are widely used to enhance the solubility of BCS class II and IV compounds. Since PROTACs often exhibit solubility issues, this could be a key step to bringing oral PROTAC formulations to the market. This study examined the manufacturing of ASDs of a model PROTAC via spray drying with different polymers. A small-scale screening method was applied and helped select polymers for the scale-up experiment. The translation of the screening results was demonstrated and the manufactured formulations were tested for stability under different storage conditions. The ASDs containing 10 % of a CRBN-based PROTAC were stable up to 40 °C over 8 weeks when protected from light and humidity. Additionally, these formulations were able to provide a very high supersaturation compared to the amorphous neat API and, interestingly, to their PM as well.

The reason for the superiority of the ASD compared to a PM of the neat, amorphous API with the corresponding polymer was investigated. The results suggest that a homogeneous distribution of the API in the polymer matrix may be needed to exhibit a high supersaturation. Additionally, for Soluplus an improved wettability of the SDD formulation compared to its physical mixture may improve the effect. However, particle size was not one of the crucial factors influencing supersaturation.

This work compliments the results from Pöstges et al. (2023) since ASDs are a useful formulation type to enhance the solubility of PROTACs. In the present study a more common approach – namely spray drying – could successfully be applied. In addition, the concept could be expanded from VHL- to CRBN-based PROTACs, demonstrating the broad applicability of ASDs for solubility enhancement of PROTACs.

CRediT authorship contribution statement

Nicole Hofmann: Conceptualization, Investigation, Formal analysis, Visualization, Writing – original draft. **Meike Harms:** Conceptualization, Supervision, Writing – review & editing. **Karsten Mäder:** Conceptualization, Supervision, Writing – review & editing.

Declaration of competing interest

The authors declare the following financial interests/personal relationships which may be considered as potential competing interests: Meike Harms reports financial support was provided by Merck KGaA. Nicole Hofmann reports financial support was provided by Merck KGaA.

Data availability

Data will be made available on request.

Appendix A. Supplementary material

Supplementary data to this article can be found online at https://doi.org/10.1016/j.ijpharm.2023.123725.

References

Attia, M.S., Elshahat, A., Hamdy, A., Fathi, A.M., Emad-Eldin, M., Ghazy, F.-E.-S., Chopra, H., Ibrahim, T.M., 2023. Soluplus® as a solubilizing excipient for poorly water-soluble drugs: Recent advances in formulation strategies and pharmaceutical product features. J. Drug Delivery Sci. Technol. 84, 104519 https://doi.org/10.1016/j.jddst.2023.104519.

Auch, C., Harms, M., Mäder, K., 2018. Melt-based screening method with improved predictability regarding polymer selection for amorphous solid dispersions. Eur. J. Pharm. Sci. 124, 339–348. https://doi.org/10.1016/j.ejps.2018.08.035.

Baghel, S., Cathcart, H., O'Reilly, N.J., 2016. Polymeric Amorphous Solid Dispersions: A Review of Amorphization, Crystallization, Stabilization, Solid-State Characterization, and Aqueous Solubilization of Biopharmaceutical Classification System Class II Drugs. J. Pharm. Sci. 105, 2527–2544. https://doi.org/10.1016/j.xphs.2015.10.008.

Baghel, S., Cathcart, H., O'Reilly, N.J., 2018. Understanding the generation and maintenance of supersaturation during the dissolution of amorphous solid dispersions using modulated DSC and 1H NMR. Int. J. Pharm. 536, 414–425. https://doi.org/10.1016/j.ijpharm.2017.11.056.

BASF Pharma, 2019. Technical information: Soluplus, 14 pp. https://pharma.basf.com/technicalinformation/30446233/soluplus (accessed 6 September 2023).

Békés, M., Langley, D.R., Crews, C.M., 2022. PROTAC targeted protein degraders: the past is prologue. Nat. Rev. Drug Discov. https://doi.org/10.1038/s41573-021-00371-6.

Bricelj, A., Steinebach, C., Kuchta, R., Gütschow, M., Sosič, I., 2021. E3 Ligase Ligands in Successful PROTACs: An Overview of Syntheses and Linker Attachment Points. Front. Chem. 9, 707317 https://doi.org/10.3389/fchem.2021.707317.

Bruner, L., Tolloczko, S., 1900. Über die Auflösungsgeschwindigkeit fester Körper. Z. Phys. Chem. 35U, 283–290. https://doi.org/10.1515/zpch-1900-3517.

Burslem, G.M., Crews, C.M., 2017. Small-Molecule Modulation of Protein Homeostasis. Chem. Rev. 117, 11269–11301. https://doi.org/10.1021/acs.chemrev.7b00077.

Burslem, G.M., Song, J., Chen, X., Hines, J., Crews, C.M., 2018. Enhancing Antiproliferative Activity and Selectivity of a FLT-3 Inhibitor by Proteolysis Targeting Chimera Conversion. J. Am. Chem. Soc. 140, 16428–16432. https://doi.org/10.1021/jacs.8b10320.

Chen, Y., Wang, S., Wang, S., Liu, C., Su, C., Hageman, M., Hussain, M., Haskell, R., Stefanski, K., Qian, F., 2016. Initial Drug Dissolution from Amorphous Solid Dispersions Controlled by Polymer Dissolution and Drug-Polymer Interaction. Pharm. Res. 33, 2445–2458. https://doi.org/10.1007/s11095-016-1969-2.

Chen, Y., Tandon, I., Heelan, W., Wang, Y., Tang, W., Hu, Q., 2022. Proteolysis-targeting chimera (PROTAC) delivery system: advancing protein degraders towards clinical translation. Chem. Soc. Rev. 51, 5330–5350. https://doi.org/10.1039/d1cs00762a.

Chokshi, R.J., Zia, H., Sandhu, H.K., Shah, N.H., Malick, W.A., 2007. Improving the dissolution rate of poorly water soluble drug by solid dispersion and solid solution: pros and cons. Drug Deliv. 14, 33–45. https://doi.org/10.1080/10717540600640278.

Churcher, I., 2018. Protac-Induced Protein Degradation in Drug Discovery: Breaking the Rules or Just Making New Ones? J. Med. Chem. 61, 444–452. https://doi.org/10.1021/acs.jmedchem.7b01272.

Cimas, F.J., Niza, E., Juan, A., Del Noblejas-López, M.M., Bravo, I., Lara-Sanchez, A., Alonso-Moreno, C., Ocaña, A., 2020. Controlled Delivery of BET-PROTACs. In Vitro Evaluation of MZ1-Loaded Polymeric Antibody Conjugated Nanoparticles in Breast Cancer. Pharmaceutics 12. https://doi.org/10.3390/pharmaceutics12100986.

Dahlberg, C., Millqvist-Fureby, A., Schuleit, M., Furó, I., 2010. Polymer-drug interactions and wetting of solid dispersions. Eur. J. Pharm. Sci. 39, 125–133. https://doi.org/10.1016/j.ejps.2009.11.005.

Dokoumetzidis, A., Macheras, P., 2006. A century of dissolution research: from Noyes and Whitney to the biopharmaceutics classification system. Int. J. Pharm. 321, 1–11. https://doi.org/10.1016/j.ijpharm.2006.07.011.

Edmondson, S.D., Yang, B., Fallan, C., 2019. Proteolysis targeting chimeras (PROTACs) in 'beyond rule-of-five' chemical space: Recent progress and future challenges. Bioorg. Med. Chem. Lett. 29, 1555–1564. https://doi.org/10.1016/j.bmcl.2019.04.030.

Efentakis, M., Al-Hmoud, H., Buckton, G., Rajan, Z., 1991. The Influence of surfactants on drug release from a hydrophobic matrix. Int. J. Pharm. 70, 153–158.

Evonik Operations GmbH, 2021. Technical information: Eudragit E 100, Eudragit E PO and Eudragit E 12,5: Specifications and Test Methods, 6 pp.

Fu, Y., Rathod, D., Patel, K., 2020. Protein kinase C inhibitor anchored BRD4 PROTAC PEGylated nanoliposomes for the treatment of vemurafenib-resistant melanoma. Exp. Cell Res. 396, 112275 https://doi.org/10.1016/j.yexcr.2020.112275.

Gottschalk, N., Bogdahn, M., Quodbach, J., 2023. 3D printing of amorphous solid dispersions: A comparison of fused deposition modeling and drop-on-powder printing. Int. J. Pharmaceut: X 5, 100179. https://doi.org/10.1016/j.ijpx.2023.100179.

Greenspan, L., 1977. Humidity fixed points of binary saturated aqueous solutions. J. Res. Nat. Bur. Stand. 81A, 89–96. https://doi.org/10.6028/jres.081A.011.

He, Y., Ho, C., 2015. Amorphous Solid Dispersions: Utilization and Challenges in Drug Discovery and Development. J. Pharm. Sci. 104, 3237–3258. https://doi.org/10.1002/jps.24541.

Ishida, T., Ciulli, A., 2021. E3 Ligase Ligands for PROTACs: How They Were Found and How to Discover New Ones. SLAS Discovery: Adv. Life Sci. R & D 26, 484–502. https://doi.org/10.1177/2472555220965528.

Kojima, T., Higashi, K., Suzuki, T., Tomono, K., Moribe, K., Yamamoto, K., 2012. Stabilization of a supersaturated solution of mefenamic acid from a solid dispersion with EUDRAGIT(®) EPO. Pharm. Res. 29, 2777–2791. https://doi.org/10.1007/s11095-011-0655-7.

Krome, A.K., Becker, T., Kehraus, S., Schiefer, A., Steinebach, C., Aden, T., Frohberger, S. J., López Mármol, Á., Kapote, D., Jansen, R., Chaverra-Muñoz, L., Hübner, M.P., Pfarr, K., Hesterkamp, T., Stadler, M., Gütschow, M., König, G.M., Hoerauf, A., Wagner, K.G., 2020. Solubility and Stability Enhanced Oral Formulations for the Anti-Infective Corallopyronin A. Pharmaceutics 12. https://doi.org/10.3390/pharmaceutics12111105.

Mares, A., Miah, A.H., Smith, I.E.D., Rackham, M., Thawani, A.R., Cryan, J., Haile, P.A., Votta, B.J., Beal, A.M., Capriotti, C., Reilly, M.A., Fisher, D.T., Zinn, N., Bantscheff, M., MacDonald, T.T., Vossenkamper, A., Dace, P., Churcher, I.,

Benowitz, A.B., Watt, G., Denyer, J., Scott-Stevens, P., Harling, J.D., 2020. Extended pharmacodynamic responses observed upon PROTAC-mediated degradation of RIPK2. Commun. Biol. 3, 140. https://doi.org/10.1038/s42003-020-0868-6.

Matteucci, M.E., Miller, M.A., Williams, R.O., Johnston, K.P., 2008. Highly supersaturated solutions of amorphous drugs approaching predictions from configurational thermodynamic properties. J. Phys. Chem. B 112, 16675–16681. https://doi.org/10.1021/jp805991f.

Neklesa, T.K., Winkler, J.D., Crews, C.M., 2017. Targeted protein degradation by PROTACs. Pharmacol. Ther. 174, 138–144. https://doi.org/10.1016/j.pharmthera.2017.02.027.

Padilla, A.M., Ivanisevic, I., Yang, Y., Engers, D., Bogner, R.H., Pikal, M.J., 2011. The study of phase separation in amorphous freeze-dried systems. Part I: Raman mapping and computational analysis of XRPD data in model polymer systems. J. Pharm. Sci. 100, 206–222. https://doi.org/10.1002/jps.22269.

Pettersson, M., Crews, C.M., 2019. PROteolysis TArgeting Chimeras (PROTACs) - Past, present and future. Drug Discov. Today Technol. 31, 15–27. https://doi.org/10.1016/j.ddtec.2019.01.002.

Pike, A., Williamson, B., Harlfinger, S., Martin, S., McGinnity, D.F., 2020. Optimising proteolysis-targeting chimeras (PROTACs) for oral drug delivery: a drug metabolism and pharmacokinetics perspective. Drug Discov. Today 25, 1793–1800. https://doi.org/10.1016/j.drudis.2020.07.013.

Pöstges, F., Kayser, K., Appelhaus, J., Monschke, M., Gütschow, M., Steinebach, C., Wagner, K.G., 2023. Solubility Enhanced Formulation Approaches to Overcome Oral Delivery Obstacles of PROTACs. Pharmaceutics 15. https://doi.org/10.3390/pharmaceutics15010156.

Puri, V., Dantuluri, A.K., Kumar, M., Karar, N., Bansal, A.K., 2010. Wettability and surface chemistry of crystalline and amorphous forms of a poorly water soluble drug. Eur. J. Pharm. Sci. 40, 84–93. https://doi.org/10.1016/j.ejps.2010.03.003.

Qian, F., Huang, J., Zhu, Q., Haddadin, R., Gawel, J., Garmise, R., Hussain, M., 2010. Is a distinctive single Tg a reliable indicator for the homogeneity of amorphous solid dispersion? Int. J. Pharm. 395, 232–235. https://doi.org/10.1016/j.ijpharm.2010.05.033.

Sakamoto, K.M., Kim, K.B., Kumagai, A., Mercurio, F., Crews, C.M., Deshaies, R.J., 2001. Protacs: chimeric molecules that target proteins to the Skp1-Cullin-F box complex for ubiquitination and degradation. Proc. Natl. Acad. Sci. USA 98, 8554–8559. https://doi.org/10.1073/pnas.141230798.

Saraswat, A., Patki, M., Fu, Y., Barot, S., Dukhande, V.V., Patel, K., 2020. Nanoformulation of PROteolysis TArgeting Chimera targeting 'undruggable' c-Myc for the treatment of pancreatic cancer. Nanomedicine (Lond.) 15, 1761–1777. https://doi.org/10.2217/nnm-2020-0156.

Savitzky, A., Golay, M.J.E., 1964. Smoothing and Differentiation of Data by Simplified Least Squares Procedures. Anal. Chem. 36, 1627–1639. https://doi.org/10.1021/ac60214a047.

Schittny, A., Huwyler, J., Puchkov, M., 2020. Mechanisms of increased bioavailability through amorphous solid dispersions: a review. Drug Deliv. 27, 110–127. https://doi.org/10.1080/10717544.2019.1704940.

Vasconcelos, T., Marques, S., das Neves, J., Sarmento, B., 2016. Amorphous solid dispersions: Rational selection of a manufacturing process. Adv. Drug Deliv. Rev. 100, 85–101. https://doi.org/10.1016/j.addr.2016.01.012.

Yang, W., Gadgil, P., Krishnamurthy, V.R., Landis, M., Mallick, P., Patel, D., Patel, P.J., Reid, D.L., Sanchez-Felix, M., 2020. The Evolving Druggability and Developability Space: Chemically Modified New Modalities and Emerging Small Molecules. AAPS J. 22, 21. https://doi.org/10.1208/s12248-019-0402-2.

Zhang, C., Han, X.-R., Yang, X., Jiang, B., Liu, J., Xiong, Y., Jin, J., 2018. Proteolysis Targeting Chimeras (PROTACs) of Anaplastic Lymphoma Kinase (ALK). Eur. J. Med. Chem. 151, 304–314. https://doi.org/10.1016/j.ejmech.2018.03.071.